VII International Conference on Computational Methods for Coupled Problems in Science and Engineering
COUPLED PROBLEMS 2017
M. Papadrakakis, E. Oñate and B. Schrefler (Eds)

APPLICATION OF LOCAL RBF COLLOCATION METHOD TO PREDICTION OF MECHANICS-RELATED PHENOMENA DURING DC CASTING OF ALUMINIUM ALLOYS

BOŠTJAN MAVRIČ* and BOŽIDAR ŠARLER*,†

*Institute of Metals and Technology
Lepi pot 11, SI-1000 Ljubljana, Slovenia
e-mail: bostjan.mavric@imt.si, web page: http://www.imt.si

†Faculty of Mechanical Engineering, University of Ljubljana
Aškerčeva 6, SI-1000 Ljubljana, Slovenia
e-mail: bozidar.sarler@fs.uni-lj.si, web page: http://www.fs.uni-lj.si

Key words: coupled fluid flow and solid mechanics, DC casting, Radial Basis Functions, Viscoplasticity, Solidification, Local Radial Basis Function Collocation Method

Abstract. A meshless local collocation method using radial basis functions (LRBFCM) has been developed to model the thermomechanical phenomena during the process of DC casting. The model uses elastic-viscoplastic constitutive relations to describe the inhomogeneous material below the coherency isotherm. It is coupled with the results of the fluid flow model, which is used to determine the computational domain and to calculate the thermal strain.

1 INTRODUCTION

Direct chill casting is a widespread technology for casting of aluminium billets and slabs, which are further used for extrusion. The achievement of high quality of the product is difficult since the thermomechanical phenomena that occur during DC casting of aluminium billets can have a significant impact on the quality of the ingot. The main defects caused by thermomechanics are hot tearing and cracking which can occur under specific stress conditions [1].

Because of the widespread use of the process in industry, a significant effort was dedicated to the development of numerical models of the process with the aim of improving the quality of the billet at optimal productivity. This resulted in many numerical models of the process, which consider several aspects of the physical problem and are stated either with the finite-element or the finite-volume method.

In recent years, a new class of methods has emerged and has started to compete with the classic discretization methods. Various meshless methods were successfully used to solve a wide spectrum of scientific and engineering problems. In contrast to the established numerical methods, the meshless methods aim to reduce the complexity of the structure associated with the node arrangement, removing the need for polygonization of the computational domain.

The LRBFCM, which is used in the present paper, has been already successfully applied to several coupled transport problems in solidification. The first were models of continuous casting of steel [2] including the influence of electromagnetic braking [3, 4]. Later on, the method was improved with a sophisticated adaptive algorithm allowing for the design of high-accuracy macrosegregation models [5].

Although the first implementations of the method dealt with solid mechanics problems [6], a lot of effort was invested into development of the method before the application of the method to the mechanical problems in metal processing. The first use was in a model of hot-rolling process, coupling the thermal transport with the large plastic deformations [7].

In this contribution we expand the mentioned efforts by developing a meshless model of thermomechancis during DC casting of aluminium alloys. The model describes the behavior of the non-homogeneous, viscoplastic material in steady state conditions. The model is one-way coupled to the results of the associated meshless heat and momentum transfer model [13]. This model supplies the thermomechanical model with the steady state values of liquid fraction, pressure, temperature and electromagnetic force. The supplied fields are used by the thermomechanical model to determine the geometry of the computational domain and the thermal strain, which is the driving term.

2 GOVERNING EQUATIONS

The thermomechanical model is stated in small-strain approximation and considers three contributions to the total strain: the elastic strain $\boldsymbol{\varepsilon}^e$, the viscoplastic strain $\boldsymbol{\varepsilon}^p$ and the thermal strain $\boldsymbol{\varepsilon}^t$. The thermal strain is the driving term of the model and is given by

$$\boldsymbol{\varepsilon}^t(T) = \boldsymbol{I} \int_{T_s}^{T} \alpha(T) \mathrm{d}T = \boldsymbol{I}\varepsilon^t, \tag{1}$$

where T_s is the solidus temperature and $\alpha(T)$ is the temperature dependent coefficient of thermal expansion. The viscoplastic strain rate

$$\dot{\boldsymbol{\varepsilon}}^p = -\boldsymbol{v}_{cast}\nabla\boldsymbol{\varepsilon}^p + \frac{3\boldsymbol{\tau}}{2\sigma_e}\dot{\varepsilon}_0(T, \boldsymbol{\sigma}). \tag{2}$$

is determined by two terms. The first term is the advection term, which is the result of the Eulerian description of the material moving with the casting velocity $\boldsymbol{v}_{cast}$ through

the computational domain. The second term describes the contribution of the viscoplastic deformation, caused by the stresses in the billet. In the expression, the stress is present in the octahedral stress tensor $\boldsymbol{\tau} = \boldsymbol{\sigma} - \boldsymbol{I}\mathrm{tr}\boldsymbol{\sigma}/3$ and the effective stress $\sigma_e = \sqrt{2\boldsymbol{\tau} : \boldsymbol{\tau}/3}$. The effective strain rate $\dot{\varepsilon}_0(T, \boldsymbol{\sigma})$ is given by

$$\dot{\varepsilon}_0(T, \boldsymbol{\sigma}) = \begin{cases} A \exp\left(-\dfrac{Q}{RT}\right)\left(\dfrac{\sigma_e}{\sigma_0}\right)^n, & \text{if } T < T_s \\ A'\left(\dfrac{\sigma_e}{\sigma_0'}\right)^{n'}, & \text{otherwise.} \end{cases} \tag{3}$$

Two variations of the Norton-Hoff's law are used to describe the behavior of the material in the mushy zone ($T_s < T < T_{coh}$) and in the solid material ($T < T_s$) as proposed in [8]. By expressing the total strain with displacement vector $\boldsymbol{u}$, the following equilibrium equation is obtained

$$\begin{aligned} 0 = & G\nabla^2\boldsymbol{u} + (G+\lambda)\nabla(\nabla\cdot\boldsymbol{u}) \\ & + \nabla\lambda(\nabla\cdot\boldsymbol{u}) + \nabla G\big(\nabla\boldsymbol{u} + (\nabla\boldsymbol{u})^T\big) \\ & - \nabla\cdot(2G\boldsymbol{\varepsilon}^p) - \nabla\big((3\lambda+2G)\varepsilon^t\big) \\ & + \boldsymbol{f}_g. \end{aligned} \tag{4}$$

The equation accounts for inhomogeneous material properties and coupling of deformation field with thermal and plastic strain. The dependence of Lame parameters λ and G on temperature is obtained from JMatPro database for the considered alloy [14]. The body force $\boldsymbol{f}_g$ is the gravitational body force.

2.1 Boundary conditions

The boundary conditions of the problem and the computational domain are illustrated in Figure 1. The problem is axisymmetric, so the cylindrical coordinate system with the coordinates (r, z) is used. The computational domain is determined by the extent of the computational domain of the heat and mass transfer model. At the top, the computational domain is limited by the position of the isoline at coherency temperature T_{coh}, above which the material cannot transfer stress and is governed by the equations of fluid dynamics.

At the coherency isoline, the material has to support the metalostatic pressure of the liquid $\boldsymbol{t} = -p\boldsymbol{n}$, where p is the pressure of the liquid calculated by the heat and momentum transfer model. The center of the billet coincides with the symmetry axis, where $u_r = 0$ and $\frac{\partial u_z}{\partial r} = 0$. At the bottom of the computational domain we set $u_z = 0$ and $t_r = 0$. The outer surface is traction free $\boldsymbol{t} = 0$ except at the top, where the contact with the mold is possible. In that area, an iterative method is used to satisfy the boundary conditions $u_r \leq 0$ and $t_r \leq 0$.

There are no specific boundary conditions for the viscoplastic strain for the most of the boundary and the rate equation is used to calculate the values on the boundary also. The

only exception to this is the top boundary, where the material is solidifying. We assume that the freshly solidified material does not accumulate any plastic strain by setting $\boldsymbol{\varepsilon}^p = 0$ at the top boundary.

3 NUMERICAL METHOD

3.1 Spatial discretization

The spatial discretization is in this contribution achieved by the LRBFCM. Elaboration of the method for linear thermoelasticity is given in [9, 10].

To formulate the method, a node arrangement is constructed with points positioned in the domain Ω and on boundary Γ. For each point in the computational domain $\boldsymbol{r}_l$ a set of nearby points, called local subdomain, is selected. The points in the subdomain are used to construct the local interpolation of the solution. The selection of the subdomain induces mapping ${}_ls(k)$, which maps the local index $k = 1, \ldots, {}_lN$ in the subdomain l to the global index in the range $1, \ldots, N$, where N is the total number of points in the node arrangement.

On each subdomain an interpolation of the unknown solution $\boldsymbol{y}$ is constructed by using multiquadrics (MQ). A MQ centered at node l is given by

$$\Phi_l(\boldsymbol{r}) = \sqrt{\frac{\epsilon^2}{h_l^2}|\boldsymbol{r} - \boldsymbol{r}_l|^2 + 1}. \tag{5}$$

Here ϵ is the shape parameter and h_i is the size of the subdomain on which the interpolation is being constructed. It is defined as

$$h_l = \sqrt{\sum_{j=1}^{{}_lN} \frac{|\boldsymbol{r}_{{}_ls(j)} - \boldsymbol{r}_l|^2}{{}_lN - 1}}. \tag{6}$$

Since MQs are only conditionally positively definite, the interpolation problem formulated solely by MQs might be ill-conditioned. The remedy is to augment the interpolation problem with m monomials $p_i(r)$, $i = 1, \ldots, m$, which constitute a basis for the polynomials of certain order. The approximation of an arbitrary field $\boldsymbol{y}$ is then given by

$$y_\xi(\boldsymbol{r}) \approx \sum_{i=1}^{{}_lN} {}_l\alpha_{i,\xi}\Phi_{{}_ls(i)}(\boldsymbol{r}) + \sum_{i=1}^{m} {}_l\alpha_{({}_lN+i),\xi}p_i(\boldsymbol{r}) = \sum_{i=1}^{{}_lN+m} {}_l\alpha_{i,\xi}\Psi_i(\boldsymbol{r}). \tag{7}$$

Here l is the index of the subdomain centered on the node closest to the evaluation point $\boldsymbol{r}$. The index $\xi = 1, \ldots, n_d$ is running over the components of the physical field that is being interpolated. In this equation the basis function $\Psi_i(\boldsymbol{r})$ is implicitly defined. It is either MQ or a monomial, depending on the value of i.

The values of the coefficients ${}_l\alpha_{i,\xi}$ are determined by solving an linear system $A\alpha = \gamma$, where the components of A are

$${}_lA_{ji,\xi\chi} = \begin{cases} \Psi_i(\boldsymbol{r}_{{}_ls(j)})\delta_{\xi\chi} & \text{if} \quad \boldsymbol{r}_{{}_ls(j)} \in \Omega \\ \mathcal{B}_{\xi\chi}(\boldsymbol{r}_{{}_ls(j)})\Psi_i(\boldsymbol{r}_{{}_ls(j)}) & \text{if} \quad \boldsymbol{r}_{{}_ls(j)} \in \Gamma \\ p_j(\boldsymbol{r}_{{}_ls(i)})\delta_{\xi\chi} & \text{if} \quad j \geq {}_lN \quad \text{and} \quad i \leq {}_lN \\ 0 & \text{otherwise} \end{cases} \tag{8}$$

and the elements of the right-hand side vector γ by

$${}_l\gamma_{j,\xi} = \begin{cases} y_\xi(\boldsymbol{r}_{{}_ls(j)}) & \text{if} \quad \boldsymbol{r}_{{}_ls(j)} \in \Omega \\ b_\xi(\boldsymbol{r}_{{}_ls(j)}) & \text{if} \quad \boldsymbol{r}_{{}_ls(j)} \in \Gamma \\ 0 & \text{if} \quad j \geq {}_lN \end{cases}. \tag{9}$$

If a point in a subdomain lies on the boundary, linear boundary conditions of the form $\sum_\xi \mathcal{B}_{\chi\xi}(\boldsymbol{r})y_\xi(\boldsymbol{r}) = b_\chi(\boldsymbol{r})$ are included in the local interpolation, forcing the local interpolation to analytically satisfy the boundary conditions.

From this construction, the result of applying a linear differential operator $\mathcal{D}$ to the local interpolation is

$$\sum_{\chi=1}^{n_d} \mathcal{D}_{\xi\chi}(\boldsymbol{r}_l)y_\chi(\boldsymbol{r}_l) \approx \sum_{k=1}^{{}_lN+m} \sum_{\chi=1}^{n_d} {}_l\gamma_{k,\chi} \sum_{i=1}^{{}_lN+m} \sum_{\zeta=1}^{n_d} {}_lA^{-1}_{ik,\zeta\chi}\mathcal{D}_{\xi\zeta}\Psi_i(\boldsymbol{r}_l). \tag{10}$$

By introducing discretization coefficients ${}_lw_{k,\xi\chi}$ given by

$${}_lw_{k,\xi\chi} = \sum_{i=1}^{{}_lN+m} \sum_{\zeta=1}^{n_d} {}_lA^{-1}_{ik,\zeta\chi}\mathcal{D}_{\xi\zeta}\Psi_i(\boldsymbol{r}_l). \tag{11}$$

this gives

$$\mathcal{D}\boldsymbol{y}(\boldsymbol{r})_\xi = \sum_{k=1}^{{}_lN+m} \sum_{\chi=1}^{n_d} {}_l\gamma_{k,\chi l}w_{k,\xi\chi}, \tag{12}$$

an expression similar to the finite-difference type of methods.

3.2 Time discretization

The viscoplastic strain rate equation causes the problem to be time-dependent and requires use of a time discretization scheme. In this paper, the implicit Euler method is used. The resulting system of nonlinear equations is solved simultaneously with the stress equilibrium equations. The unknowns are u_r, u_z, ε^p_{rr}, ε^p_{rz}, ε^p_{zz} and $\varepsilon^p_{\phi\phi}$.

To obtain the solution, Bouaricha tensor method is used. The linear solves required by the method are performed by FGMRES preconditioned by PARDISO solves with Jacobian that is evaluated at the start of each time step.

Casting parameter	Value
Melt temperature	730 °C
Casting speed	80 mm/min
DC water temperature	20 °C
DC water flux	7 m^3/h

Table 1: Casting parameters used in HMTM of DC casting of Al-Cu alloys.

Law parameter	Value
A	$9 \cdot 10^5\,s^{-1}$
Q	$145\,kJ/kg$
n	3.8
σ_0	4 MPa
A'	$10^{-6}\,s^{-1}$
n'	4
σ_0'	1 MPa

Table 2: Parameters of the viscoplastic constitutive law given by equation (3).

4 RESULTS

The unknown displacement vector and viscoplastic strain are the primary results of the model. They are illustrated in figures 2 and 3 for the Al 4% Cu alloy. The material properties and process parameters are given in tables 2 and 1, respectively. The plots in the figures demonstrate the typical results of the model.

Because of the thermal contraction, the component u_r is negative throughout the billet, except for a thin strip at the top of the mushy zone. The component negative values of u_z are caused by thermal contraction and the gravitational force, combined with the fact that the z coordinate of the bottom boundary is kept fixed.

The components of the plastic strain have a more complicated spatial dependence. Most of the changes occur in the mushy zone or immediately below it. No changes of the plastic strain components outside this area are the result of the exponential damping of the viscoplastic strain rate as temperature decreases. Below this area, the r profiles of the stress components dependence remain constant.

The impact of the mold contact can be seen in the plots of components ε^p_{rr} and ε^p_{zz} in figures 3a and 3b, respectively. The thin strip of high plastic strain at the top of the mushy zone near the outer surface of the billet is caused by the compressive forces caused by the melt pressure. They result in compressive strain in the r direction and extension in the z direction because of the volume-preserving nature of the plastic flow.

By studying the profile of ε^p_{rz} shown in Figure 3d, we can gain insight on the conditions that are experienced by the material as it travels through the computational domain. Lets track a thin ring of material with radius $r = 0.1$ m. The material in the ring becomes coherent at $z = -0.10$m. and starts to move downwards with the casting velocity. As it solidifies, it is positioned on the innermost part of the solid shell. The outer surface of the shell is cooled as it moves downwards, causing it to contract. This contraction puts the observed ring under compressive stress in circumferential direction, forcing it to contract. As enough material is accumulated on the inside of the shell, the observed ring changes its role. It starts to cool faster that the newly accumulated solid on the interior, which

results in it being subjected to tensile stress conditions. This results in the increase in the plastic strain, which can only go on while the ring is at high enough temperature in the area above $z = -0.25$ m. Below this position, the strain remains constant, since the stresses there are too small to cause the plastic deformation.

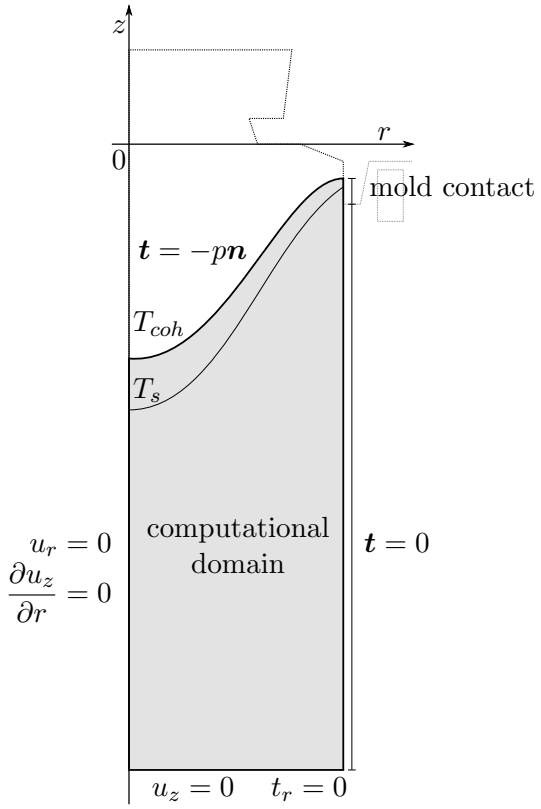

Figure 1: Geometry of the DC casting model and the boundary conditions.

5 CONCLUSIONS

The model presented in this paper is capable of modeling the viscoplastic stress and strain during the process of DC casting. The model couples the thermomechanical model of a viscoplastic solid with the steady state results from the model of heat and mass transfer. The results given in terms of displacement and viscoplastic strain show the behavior expected from the casting practice.

In the future, the model will be used to analyze the effect of casting parameters on hot-tearing susceptibility and on formation of porosity.

ACKNOWLEDGMENTS

The research presented in this paper was funded by the Young Researcher program by Slovenian Ministry of Higher Education, Science and Sport and by companies Impol,

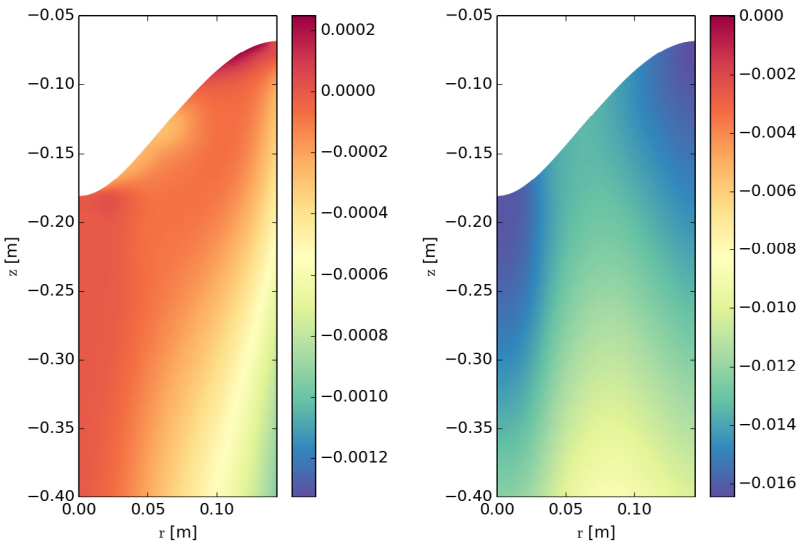

(a) u_r **(b)** u_z

Figure 2: Displacement field.

Slovenska Bistrica and Štore Steel.

REFERENCES

[1] Eskin, D.G. *Physical Metallurgy of Direct Chill Casting of Aluminum Alloys*. Taylor & Francis, (2008).

[2] Vertnik, R. and Šarler, B. Simulation of continuous casting of steel by a meshless technique *International Journal of Cast Metals Research* (2009) **22**:311–313.

[3] Mramor, K. and Šarler, B. A meshless model of electromagnetic braking for the continuous casting of steel *Materials and Technologies* (2015) **49**:961–967.

[4] Mramor, K., Vertnik, R. and Šarler, B. Low and intermediate Re solution of lid driven cavity problem by local radial basis function collocation method *CMES: Computer Modeling in Engineering & Sciences* (2013) **92**:327–352.

[5] Kosec, G., Založnik, M., Šarler, B. and Combeau, H. A meshless approach towards solution of macrosegregation phenomena *Computers, Materials and Continua* (2011) **22**:169–195.

[6] Lee, C. K., Liu, X. and Fan, S. C. Local multiquadric approximation for solving boundary value problems *Computational Mechanics* (2003) **30**:396–409.

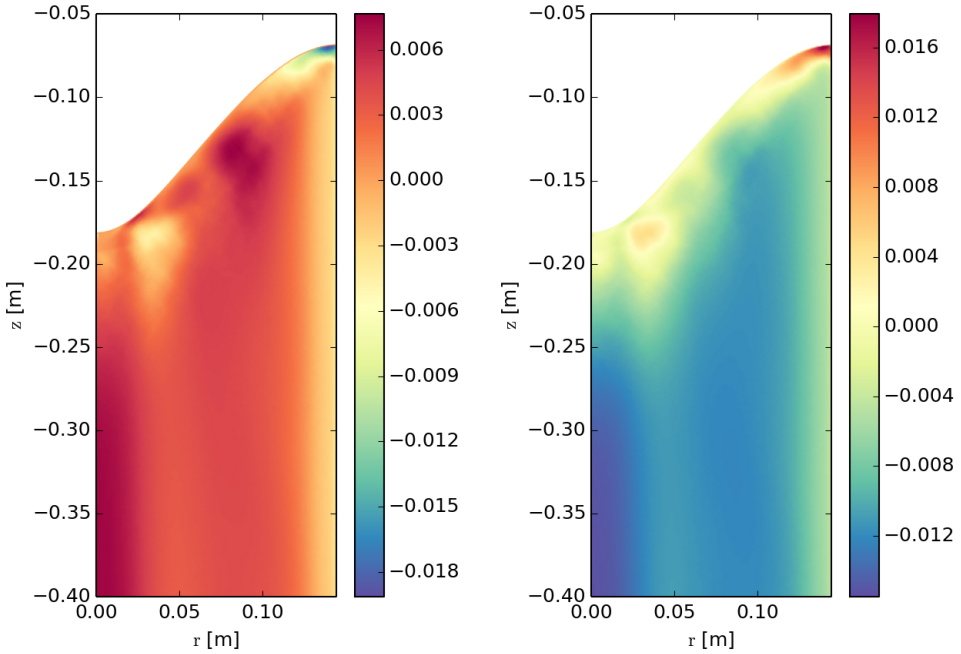

(a) ε^p_{rr} **(b)** ε^p_{zz}

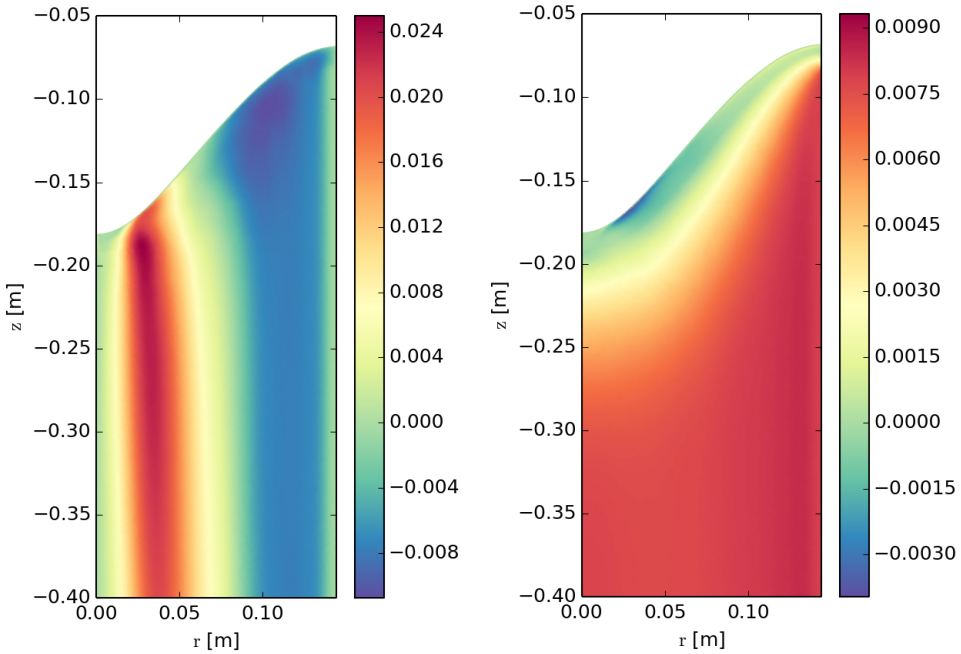

(c) ε^p_{rz} **(d)** $\varepsilon^p_{\phi\phi}$

Figure 3: Viscoplastic strain.

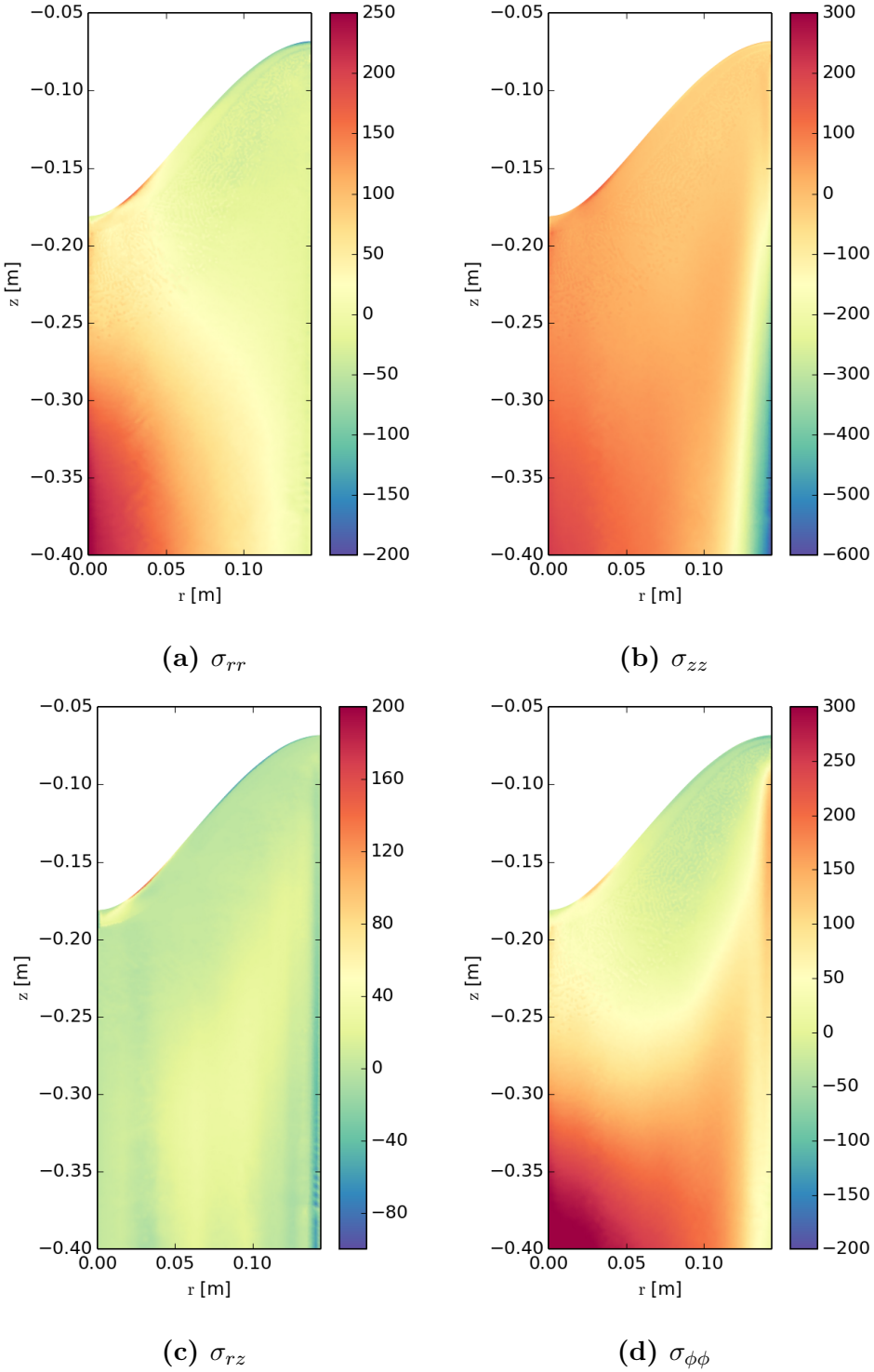

(a) σ_{rr} **(b)** σ_{zz}

(c) σ_{rz} **(d)** $\sigma_{\phi\phi}$

Figure 4: Stress tensor components in MPa.

[7] Hanoglu, U. and Šarler, B. Simulation of Hot Shape Rolling of Steel in Continuous Rolling Mill by Local Radial Basis Function Collocation Method *CMES: Computer Modeling in Engineering & Sciences* (2015) **109**:447–479.

[8] Nallathambi, A. K., Tyagi, M., Specht, E. and Bertram, A. Thermomechanical simulation of direct chill casting *Transactions of The Indian Institute of Metals* (2011) **64**:13–19.

[9] Mavrič, B. and Šarler, B. Local radial basis function collocation method for linear thermoelasticity in two dimensions *International Journal of Numerical Methods for Heat & Fluid Flow* (2015) **25**:1488–1510.

[10] Mavrič, B. and Šarler, B. Application of the RBF collocation method to transient coupled thermoelasticity *International Journal of Numerical Methods for Heat & Fluid Flow* (2017) **27**(5).

[11] Ludwig, O., Drezet, J. M., Martin, C. L. and Suery, M. Rheological behavior of Al-Cu alloys during solidification constitutive modeling, experimental identification, and numerical study *Metallurgical and Materials Transactions A* (2005) **36**:1525–1535.

[12] Suyitno, O., Kool, W. H. and Katgerman, L. Integrated Approach for Prediction of Hot Tearing *Metallurgical and Materials Transactions A* (2009) **40**:2388–2400.

[13] Hatić, V., Mavrič, B., Košnik, N., and Šarler, B. Simulation of direct chill casting under the influence of a low-frequency electromagnetic field *Applied Mathematical Modelling* (2017) (accepted).

[14] Saunders, N., Guo, U. K. Z., Li, X., Miodownik, A. P. and Schillé, J.-Ph. Integrated Approach for Prediction of Hot Tearing *JOM* (2003) **55**:60–65.